Supporting Information

Substitution boosts charge separation for high solar-driven photocatalytic performance

Gong Zhang[a, e†], Le Zhang[d†], Yang Liu[b], Limin Liu[d], Chin-Pao Huang[c], Huijuan Liu[*a, e], and Jinghong Li[*b]

[a] State Key Laboratory of Environmental Aquatic Chemistry, Research Center for Eco-Environmental Sciences, Chinese Academy of Sciences, Beijing 100085, China

[b] Department of Chemistry, Key Laboratory of Bioorganic Phosphorus Chemistry & Chemical Biology, Beijing Key Laboratory for Microanalytical Methods and Instrumentation, Tsinghua University, Beijing 100084, China.

[c] Department of Civil and Environmental Engineering, University of Delaware, Newark, DE 19716, USA

[d] Beijing Computational Science Research Center, Beijing 100084, China

[e] University of Chinese Academy of Sciences, Beijing 100039, China

*Corresponding Author

hjliu@rcees.ac.cn

jhli@mail.tsinghua.edu.cn

This Supporting Information Contains the Following Sections:

Supplementary Note

ICP-OES and ion chromatography measurements

The sample was prepared by dissolving the 10 mg $BiOBr_aI_b$ in a concentrated oxalic acid solution followed by diluting to 1 L with distilled water. The amount of Bi was detected using its emission line at 223.06 nm in an Agilent ICP-OES, and the Bi standard (1000 mg L^{-1}) was diluted to 1.0, 2.5, 5.0, and 10.0 mg L^{-1} as calibration. The amount of Br or I was inspected in a Dionex ion chromatography. The concentration of bromide (Br^-) or iodide (I^-) was measured by the conductivity detector. Separation of the two halide ions was conducted using an Ion Pacs AS19 ion chromatography column (4×250 mm) with an Ion Pacs AG19 (4×50 mm) guard column (Dionex). The mobile phase was generated using a potassium hydroxide eluent generator at a flow rate of 1.0mL min^{-1}.[1]

Supplementary Figures:

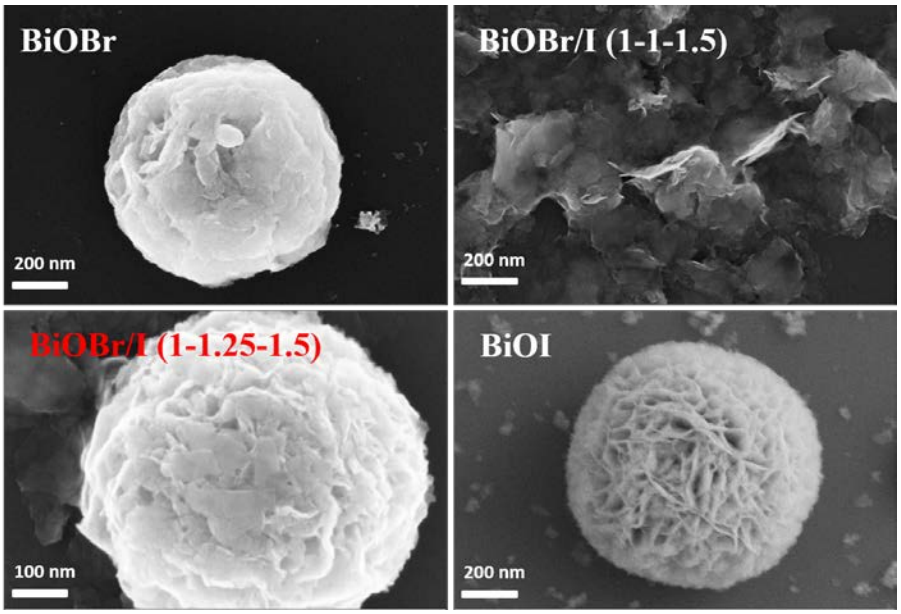

Figure S1. SEM images of BiOX samples fabricated using solvothermal method. As observed, without substitution, BiOBr and BiOI microspheres could be obtianed. With adding different amount of precursors, the photocatalst demonstrate the different physical structures, ranging from flake to irregular solid sphere.

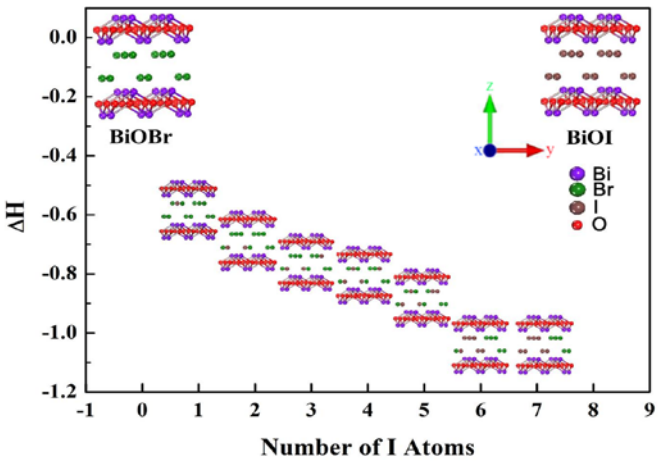

Figure S2. The calculated reaction enthalpy values of BiOBr crystal with different numbers of iodine substitution. The minus values indicate that stable structure could be achieved with arbitrary substitution of iodine atoms into BiOBr.

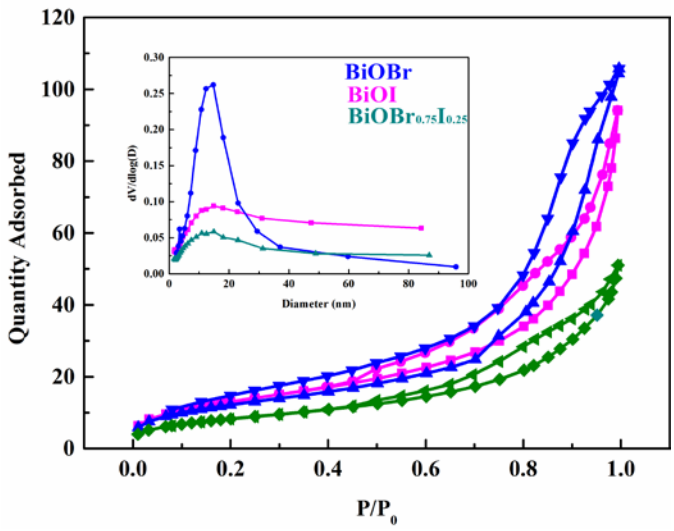

Figure S3. The BET analyses of the BiOBr, BiOI, and $BiOBr_{0.75}I_{0.25}$.

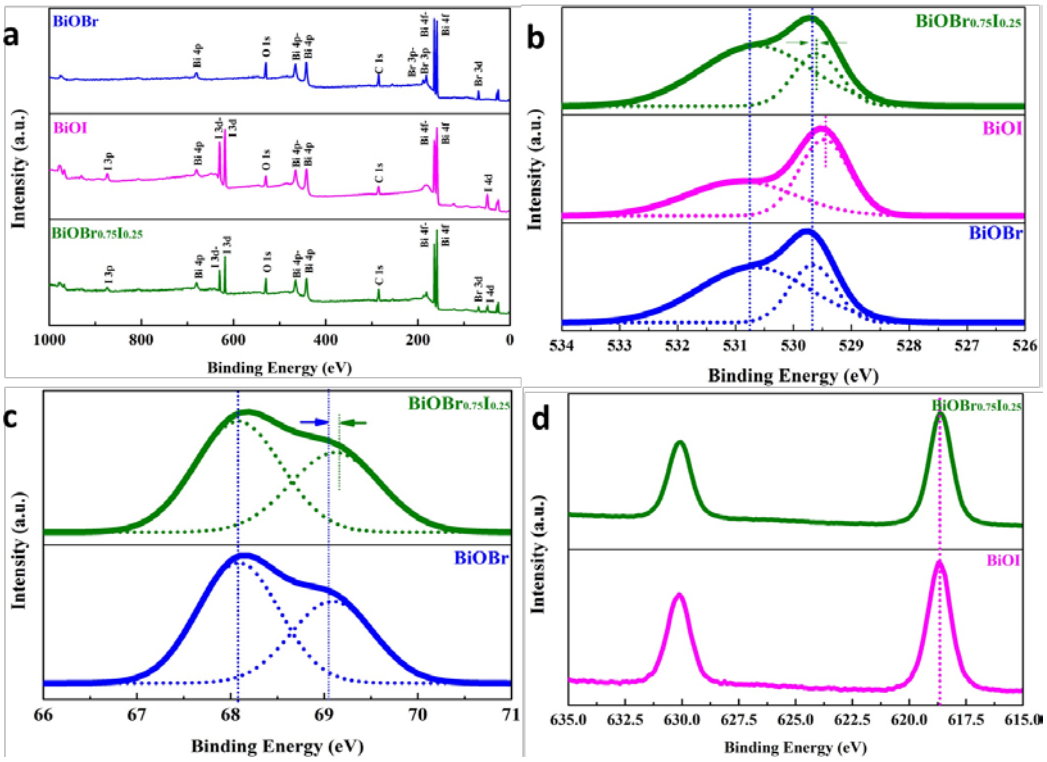

Figure S4. X-Ray photoelectron spectra: (a) full scan, (b) O 1s, (c) Br 3d and (d) I 3d regions of BiOBr, BiOI and $BiOBr_{0.75}I_{0.25}$. The peaks of Bi 4f, Br 3d, I 3d, O 1s with adventitious C 1s can be observed in XPS. In contrast to BiOBr, the binding energy of Br 3d in $BiOBr_{0.75}I_{0.25}$ is red-shifted by 0.3 eV, while the peak of I $3d_{3/2}$ remains at 618.7 eV with respect to BiOI, which indicates the change of electronic landscape in the bromine atom after iodine substitution.

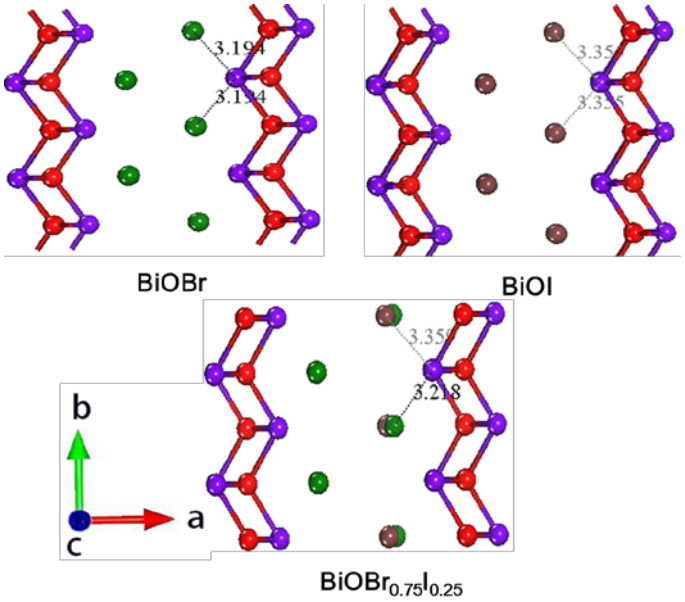

Figure S5. The atomic arrangements in BiOBr, BiOI and $BiOBr_{0.75}I_{0.25}$ based on the quantitative analysis of EXAFS regions. In contrast to BiOBr, the increased distance between Bi and Br (Supplementary Table S2) might be attributed to the electrostatic repulsion induced by the iodine atoms with smaller charge-to-mass ratio in $BiOBr_{0.75}I_{0.25}$. On the contrary, due to larger inertia, the Bi-I coordination was almost the same as that in BiOI.

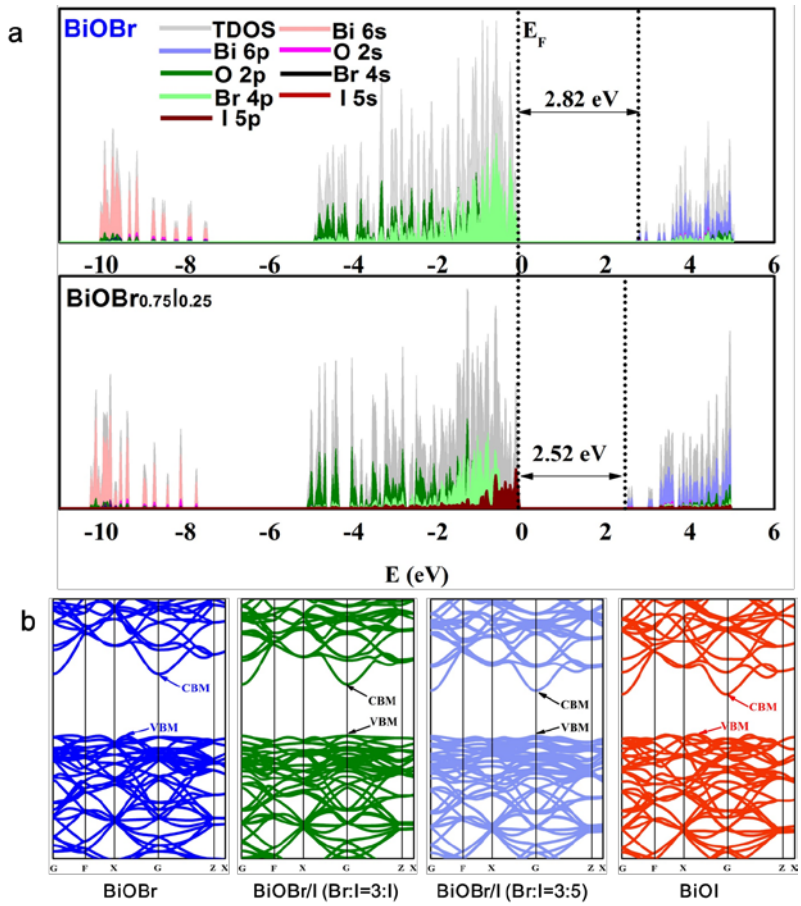

Figure S6. (a) The density of electronic states of the BiOBr and $BiOBr_{0.75}I_{0.25}$. (b) The band structure for subustitution of differnt numbers of iodine atoms into BiOBr.

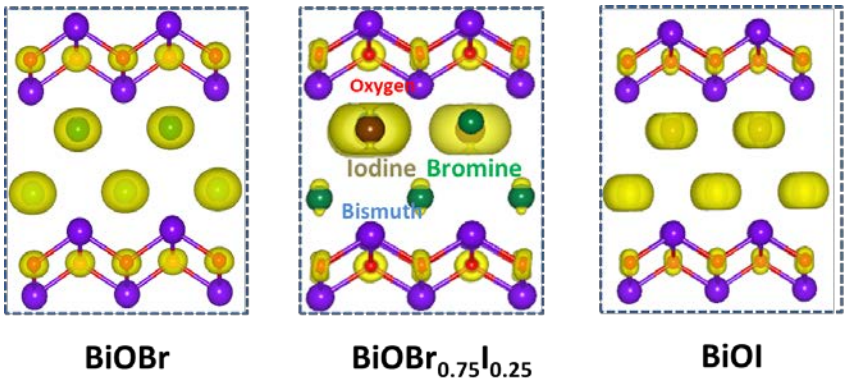

Figure S7. Electron density contour maps for the BiOBr, BiOI and $BiOBr_{0.75}I_{0.25}$. After substitution, the features of the covalent bond between bismuth and halogen atoms become stronger in $BiOBr_{0.75}I_{0.25}$ with respect to the BiOBr or BiOI, which resulted in the enhanced dipole moment of 2.98D for $BiOBr_{0.75}I_{0.25}$ in contrast to 1.70D, 2.45D that in BiOBr and BiOI.

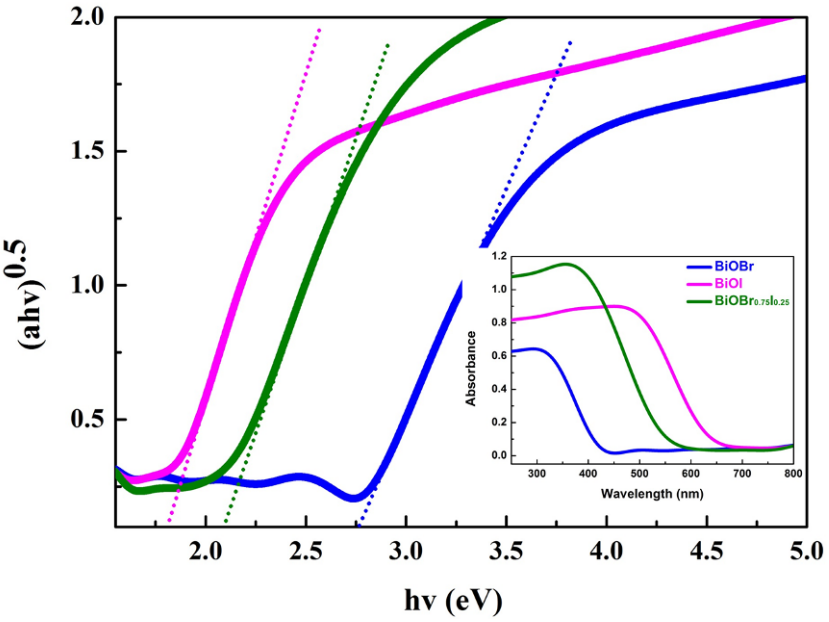

Figure S8. The diffuse reflection spectra (inset) and corresponding Tauc plots of the BiOBr, BiOI and $BiOBr_{0.75}I_{0.25}$. The BiOBr, BiOI, and $BiOBr_{0.75}I_{0.25}$ possess the bandgap of 2.75, 1.82 and 2.01 eV, which are in well agreement with the results of calculation.

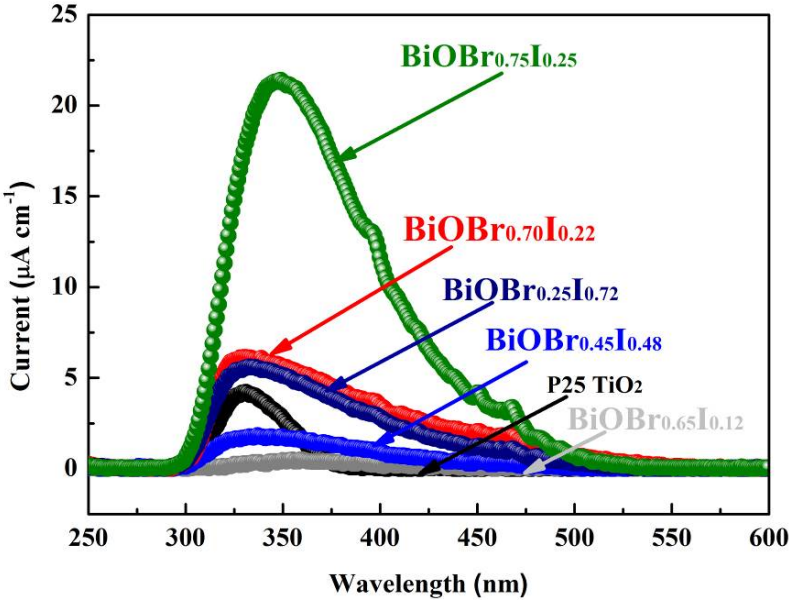

Figure S9. Photon-to-current conversion efficiencies of the BiOBr substituted by different iodine atoms were measured by photocurrent action spectra under UV and visible light. The $BiOBr_{0.75}I_{0.25}$ has much higher photon to current conversion than the others, which is due to the smallest m^*_e and largest m^*_h according to the effective mass approximations.

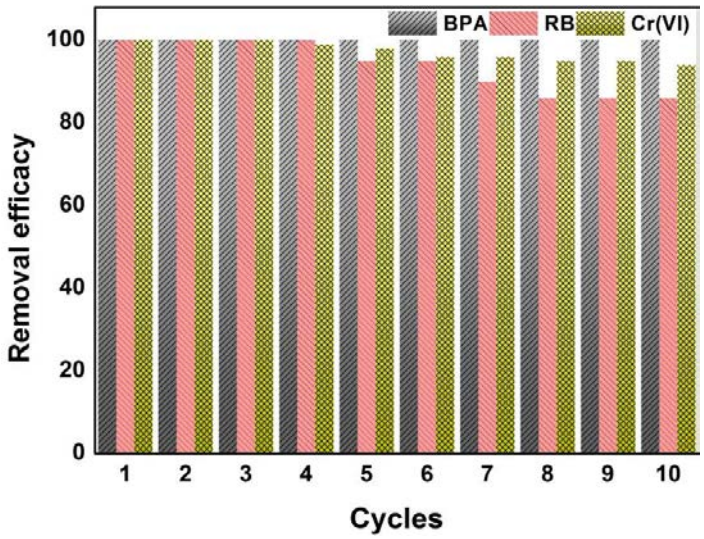

Figure S10. Photocatalytic efficiency to the chemical-containing solutions with $BiOBr_{0.75}I_{0.25}$ in differnt cycles. For every circle, after photocatalytic reaction 5 min, 20 min, and 30 min for RB, BPA and Cr^{VI}, the samples were then taken and centrifuged to separate the supernatant from the catalysts for analysing the residual concentration.

Supplementary Tables:

Table S1. Curve fitting results of Bi L-edge EXAFS.

Sample	Shell	CN [a]	R [b] (Å)	σ^2 [c] (10^{-3} Å^2)	R factor (%)
BiOBr	Bi-O	3.8±0.5	2.26	3.5	1.0
	Bi-Br	3.7±0.3	3.19	7.6	
BiOI	Bi-O	3.8±0.6	2.27	4.1	2.0
	Bi-I	3.6±0.8	3.35	8.5	
$BiOBr_{0.75}I_{0.25}$	Bi-O	3.9±0.5	2.29	3.2	1.6
	Bi-Br	2.2±0.2	3.23	7.3	
	Bi-I	1.4±0.6	3.35	8.2	

[a] CN: coordination number. [b]R: bond distance. [c] σ: Debye-Waller factor.

Note: Data were analyzed using Athena and Artemis from IFeffit 1.2.11 software package. EXAFS oscillation χ(k) was extracted by using spline smoothing with a Cook-Sayers criterion, and k2-weighted χ(k) was Fourier-transformed into R space in the k ranges of 2-10 Å for the Bi L edge with a Hanning function window. In the curve-fitting step, the backscattering amplitude and phase shift were calculated using the FEFF8.4 code. For standard samples, coordination numbers (CN), bond lengths (R), edge corrections (ΔE), and Debye-Waller (DW) factors were all set to be adjustable.

Table S2. Fitted values of the EIS data in Figure 4d

Sample	R_s (Ω cm^{-2})	C_{bulk} (F cm^{-2})	$R_{traping}$ (Ω cm^{-2})	C_{trap} (F cm^{-2})	R_{ct} (Ω cm^{-2})
BiOBr	28.1	6.8×10^{-6}	4580	4.7×10^{-5}	24896
BiOI	26.8	8.5×10^{-6}	4321	6.1×10^{-5}	8963
$BiOBr_{0.75}I_{0.25}$	28.6	5.1×10^{-5}	898	4.9×10^{-4}	2967

Supplementary References

1 Hua, G. H. & Reckhow, D. A. Determination of TOCl, TOBr and TOI in drinking water by pyrolysis and off-line ion chromatography. *Anal. Bioanal. Chem.* **2006**, 384, 495.